Integrated Piezo-Triboelectric Nanogenerators Based Self-powered Flexible Temperature and Pressure Sensor

Guanbo Min[a], Gaurav Khandelwal[a], Abhishek Singh Dahiya[a], Daniel M. Mulvihill[b] and Ravinder Dahiya[a]*
[a]Bendable Electronics and Sensing Technologies (BEST) Group,
[b]Materials and Manufacturing Research Group,
James Watt School of Engineering, University of Glasgow, Glasgow G12 8QQ, UK
*Correspondence to: Ravinder.Dahiya@glasgow.ac.uk

***Abstract* — Efficient harvesting of ubiquitous ambient mechanical energy using various types of nanogenerators (NGs) has attracted considerable interest in recent years. Herein, we present a textile triboelectric nanogenerator (T-TENG) using Polytetrafluoroethylene (PTFE) and Nylon based counter-surfaces in fabric form (both fixed to conductive fabric electrodes). T-TENG performance is enhanced by exposing PTFE film with Argon plasma. The output voltage of the plasma treated devices increased by a factor of ~10, and their short circuit current density increased by a factor of ~9 (compared to pristine non-plasma treated devices). Additionally, we demonstrate that the fabricated T-TENG can be used as a self-powered temperature sensor, tested in the 25-90 °C range. The T-TENG output voltage decreased linearly with increasing temperature exhibiting a sensitivity of ~ 1%/(°C). Further, we integrated a flexible piezoelectric nanogenerator (PENG) on top of the T-TENG to detect the contact forces. The PENG output is also used to compensate the pressure dependent output of TENG underneath, and allows distinct temperature and pressure measurements. The excellent results observed here show the potential of T-TENGs for use as self-powered sensors in applications such as health monitoring, wearables and interactive systems.**

Index Terms* — *electronic textile; triboelectric nanogenerator; piezoelectric nanogenerator; temperature; self-powered sensors

I. INTRODUCTION

Wearable and flexible electronics have gained significant interest recently because of the wide range of solutions they enable for applications such as health monitoring, robotics, displays and interactive systems etc. [1-6]. Energy autonomy is critical for these systems, especially where portability is necessary. For this reason, there is need for reliable and continuous energy sources, preferably in a flexible/wearable form factors [7, 8]. Currently the energy requirements of these systems are met through batteries, which come with drawbacks such as bulkiness, non-flexibility, use of toxic electrolytes, and limited lifespan etc. This has triggered immense interest in flexible and efficient nanogenerators (NGs) to scavenge energy from ambient green sources [9, 10].

One of these energy harvesters is the Triboelectric NGs (TENGs) which holds good potential both as an energy generator and as a self-powered sensor [11]. These devices can exploit the real contact area [12], differences in electron affinities of the interface pair [13], permittivity of the tribo-contact materials [14], and surface functionalization etc. to modulate the output and hence develop different types of self-powered devices [15, 16] [17] [18]. For example, defluorination during Argon (Ar) plasma treatment of PTFE surface can increase its surface potential [19][20-22]. Likewise, the pressure can change the real contact area between the interface pair [12, 23, 24] and the temperature can influence the material permittivity and effective density of traps [25]. The correlation of TENG output to the intensity of external stimuli, endows TENG based sensors with the feature of being 'self-powered'. Because of high efficiency, simple device design and cost effectiveness, TENGs with flexible and wearable form factors find applications in a variety of growing areas such as wearable electronics, health monitoring, IoTs, rehabilitation, motion and gas sensing, and implantable biomedical devices [26-29] [30].

Fabric-based materials have also been explored to realize wearable textile triboelectric nanogenerators (T-TENGs). However, owing to the small overall real contact area generated in fabric-fabric interfaces, the output of T-TENGs is inferior to the dielectric film-based devices. Smart designs are needed to improve their output as well as the ability to simultaneously detect multiple types of stimuli – for example, temperature and pressure. TENGs offer high sensitivity for temperature sensing but it remains a challenge to transfer the technology to wearable applications [31]. This is because the output of a TENG based temperature sensor is also affected by the change in applied force/pressure [25, 31]. Especially, when TENG based

This work is supported by Engineering and Physical Sciences Research Council through grant ref. number EP/V003380/1.

An earlier version of this paper was presented at 2022 IEEE International Conference on Flexible and Printable Sensors and Systems (FLEPS) (DOI: 10.1109/FLEPS53764.2022.9781506). (Corresponding author: Ravinder.Dahiya@glasgow.ac.uk)

G. Min, G. Khandelwal, A. S. Dahiya and R.S. Dahiya are with Bendable Electronics and Sensing Technologies (BEST) Group, University of Glasgow, G12 8QQ, UK

D.M. Mulvihill is with the Materials and Manufacturing Research Group, University of Glasgow, G12 8QQ, UK.

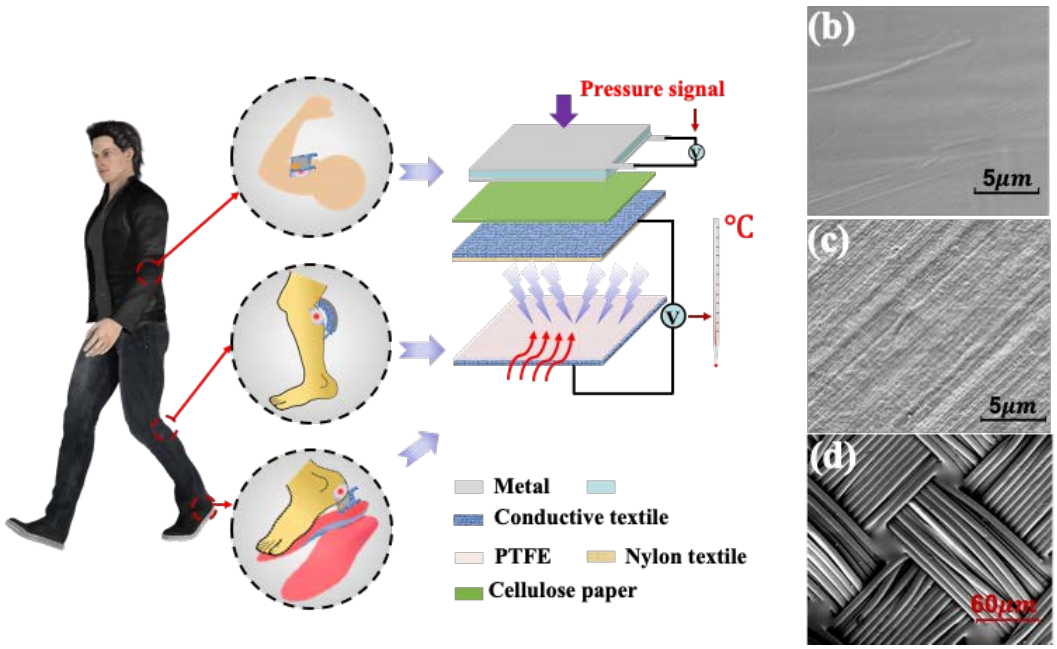

Fig. 1: (a) Schematic diagram for the proposed wearable multifunctional self-powered sensor system. The SEM images on the right correspond to (b) pristine PTFE surface, (c) Ar plasma treated PTFE surface, and (d) nylon fabric textile surface.

temperature sensors are attached onto the human body to detect skin temperature, it is difficult to distinguish the variation in outputs [32, 33]. Herein, we present a solution to this challenge by developing an integrated Piezo-Triboelectric Nanogenerator device. This paper extends the preliminary results presented at IEEE FLEPS 2022 [34], where we showed that the T-TENG can be used as a self-powered temperature sensor. The temperature sensitivity of the T-TENG was calculated using the output voltage response (i.e., $(V_0\text{-}V)/V_0$) versus temperature plots. Here, we present the multifunctional sensor system by integrating the fabricated T-TENG and a piezoelectric nanogenerator (PENG). In this structure, the T-TENG detects variation in temperature and the PENG can monitor the value of applied pressure. Any pressure related variation in T-TENG output voltage can be compensated with PENG output and hence the former can be used to precisely identify the temperature. The temperature sensitivities of the T-TENG at different pressures are calculated using the output voltage versus temperature plots.

This paper is organized as follows: The design and fabrication of the integrated device is presented in Section II. This is followed by T-TENG temperature sensing device characterization in Section III. Finally, the key outcomes of the study are summarized in Section IV.

II. Experimental

A. Design of the integrated T-TENG and PENG

Fig. 1 shows the design of a multifunctional sensor system integrating a T-TENG sensor with a PENG. The PENG can monitor the value of applied pressure on the device and the T-TENG can be used to sense variation in temperature in this design. Any pressure related variation in T-TENG output voltage can be compensated with PENG output and hence the former can be used to precisely identify the temperature. However, as PENG output is also affected by the temperature, a layer of cellulose paper is implanted between the PENG layer and T-TENG top tribo-layer as shown in Fig. 1(a). Thus, the output of the PENG remains stable at different temperatures.

B. Fabrication of T-TENG

Fig. 1 shows a schematic diagram of the fabricated T-TENG for operation in vertical contact separation mode. In the first T-TENG (Fig. 1a), the tribo-contact layers consist of a 100 μm PTFE sheet (Good fellow, UK) and a Nylon fabric textile (UKFabrics, UK). PTFE and Nylon were selected as the interface pair, because of their large difference in triboelectrification properties [44]. The PTFE surface was exposed to plasma to create nanopatterns (due to etching) to increase the surface to volume ratio (i.e., higher contact area between the interface pair). To allow optimization, the Ar plasma power was fixed at 150 W (10 mL/cc) while time was varied from 3 to 12 min (with steps of 3 min). A layer of Nylon fabric was used as a tribo-positive layer, as shown in Fig. 1(a). Note also that the conductive fabrics were used as the device electrodes. Two layers of conductive textile (Ni/Cu polyester) were attached onto the PTFE and Nylon textile sides as the electrodes. To avoid a bulge from the electrodes, they were positioned at opposite edges. The nominal contact area of each device was 2.5 × 2.5 cm^2.

C. Fabrication of PENG

A commercial metal coated P(VDF-TrFE) film (Piezotech, France) was used for fabrication of the PENG device. The thickness of the PVDF-TrFE layer was 100μm.

D. Characterization and testing

The test rig used for evaluation of the T-TENG (in normal contact separation mode) is the same as the one explained

elsewhere [35]. Prior to testing, a pre-load was applied to make contact and to self-align the surfaces. The alignment is then 'locked-in' by tightening lock screws. The mechanical movements for the T-TENGs were generated by an electrodynamic shaker system (TIRA, TV 50018, Germany), which was set to apply 8 N force at 8 Hz frequency. This produced a nominal contact pressure of 12.8 kPa. Mechanical oscillation was configured with a 2 mm max separation distance (i.e., peak-to-peak amplitude of 2 mm). The output voltage was recorded by an oscilloscope (MSO-X 4154A, Keysight, USA). To measure the output current, the oscilloscope was coupled with an inverting current to voltage converter, which consisted of a 100 kΩ feedback resistor and a LMC6001 operational amplifier (ultra-input current amplifier). Transferred charges were measured by an electrometer (Keithley 6517B, USA).

For temperature measurements, the PTFE tribo-layer was heated using a hotplate. A thermal imager (FiS20, FLUKE) was used to measure the temperature of the tribo-layer. The surface morphology of T-PTFE (see Fig. 1(b-c)) and nylon fabric textile (see Fig. 1(d)) were characterized by FEI field emission scanning electron microscope (FE-SEM). COMSOL Multiphysics 5.3 was used for simulating the device output characterizations.

III. Results and Discussion

A. Characterization of T-TENG

Fig. 2(a-d) show the output performance of the T-TENG devices; namely, output voltage (Fig. 2a), short circuit current density (Fig. 2b), transferred charges (Fig. 2c), and output power of the optimum T-TENG under different resistive loads (Fig. 2d). The T-TENG output increased as we moved from the pristine PTFE sample to the 12 min Ar plasma treated PTFE based device. The peak positive output voltage increased from 9 V (pristine – 0 min case) to 37 V (3 min case) to 61V (6 min case) to 82 V (9 min case) to 92 V (12 min case), i.e., 10.2 times enhancement from pristine to 12 min Ar plasma treated case. The output of the 12 min Ar plasma treated device is comparable with previous works (see Table I). Textile based TENGs produce low power compared to their film-based counterparts because of the low real contact area between the interface pair. In Fig. 2 (b), the peak short circuit current density was about 0.12 μA/cm^2 for the pristine case (0 min) and a maximum of 1.14 μA/cm^2 for the 12 min Ar plasma treatment case representing 9.2 times increase. A similar trend is seen in Fig. 2c for the transferred charges. The maximum output power density of the 12 min Ar plasma treatment device is 0.5 W/m^2 (Fig. 2d). The comparison of our result with previous works

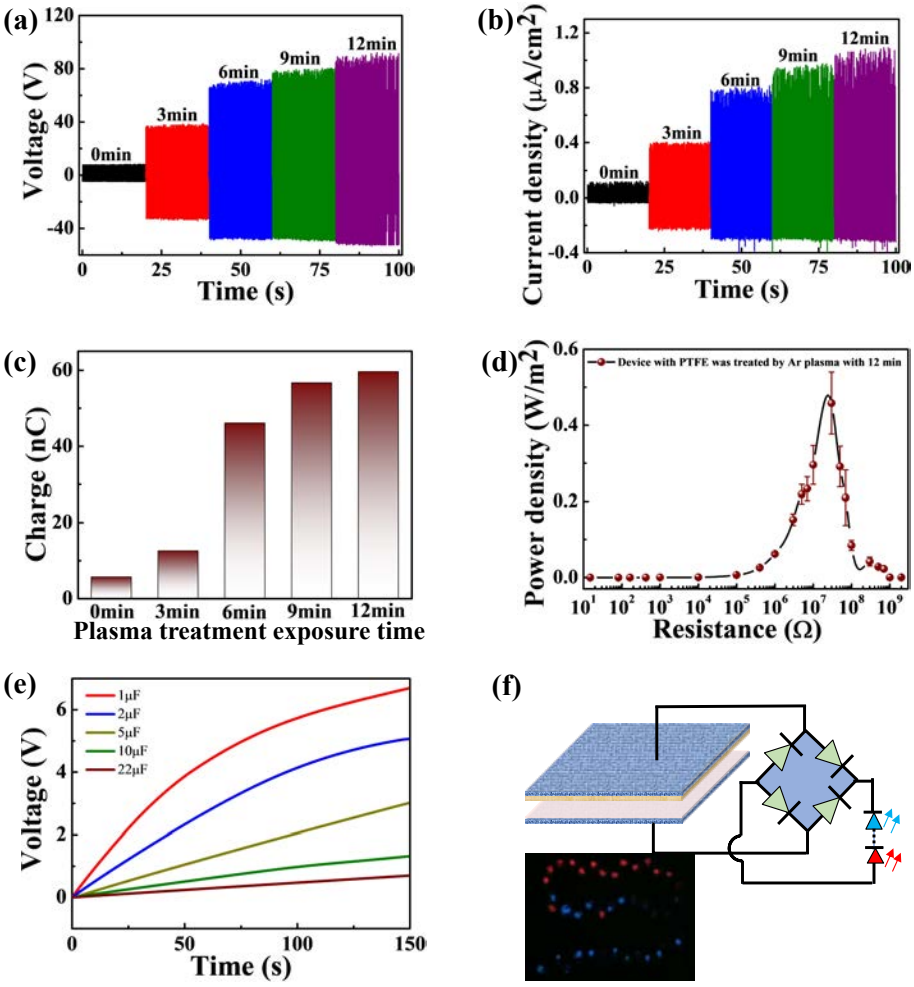

Fig. 2: (a) Characterization of device based on Ar plasma treated PTFE and Nylon textile: (a) output voltage, (b) short circuit current density, (c) transferred charges and (d) output power density, (e) voltage charging profiles for various capacitors under operating conditions of 8N and 8Hz and (f) representative energy harvesting circuit for powering LED array.

Table I. Typical PTFE based TENG performances compared with the present work (final row).

Contact materials	Pressure (kPa)	Frequency (Hz)	V_{out} (V)	J_{sc} (μA/cm^2)	Sample size (cm^2))	Ref.
Ar plasma treated PTFE & Al	0.625	5	40	0.1875	16	[19]
plasma treated PTFE & Al	33	6	30	0.083	9	[36]
PTFE & PVDF	-	4	49	1.1	18	[31]
ZnO-PVDF & PTFE	-	0.5	66	0.25	-	[35]
PTFE textile & Nylon	-	2	9.5	0.32	25	[37]
Cellulose nanofiber and FEP	-	5	22	1.21	0.6	[38]
PA6 & PTFE	-	2	80	0.25	16	[39]
Ag & PTFE	-	2	23.5	0.0105	100	[40]
PET & Nylon fabric	-	1	90	0.05	20	[41]
Ar plasma treated PTFE & Nylon fabric	**12.8**	**8**	**92**	**1.14**	**6.25**	**This work**

using similar materials is given in Table I: namely, with an Ar plasma treated PTFE based device in contact with Aluminum in [36] and a PTFE based device in contact with Nylon in [37]. The former achieved a maximum current density and output voltage of 0.083 μA/cm^2 and 30 V at a contact pressure of 33 kPa and the latter reported a maximum of 1.1 μA/cm^2 and 49 V. The present work has produced significantly higher output (1.1 μA/cm^2 and 92 V) at a lower contact pressure of 12.8 kPa. In fact, 1.14 μA/cm^2 and 92 V is among the highest values in Table I. Based on these results, we selected the 12 min Ar plasma treated PTFE layer for investigation of temperature sensing capability.

Additionally, to demonstrate device's ability to harvest energy and power electronic devices, the T-TENG was used to charge five capacitors with capacitances of 1, 2, 5, 10 and 22μF via a rectifier circuit shown in Fig. 2(f). The output in Fig. 2(e) shows an obvious trend of increasing voltage (fixed charging time) with decrease in capacitance. Finally, the T-TENG was used to power an array of 40 LEDs, as shown in Fig. 2(f).

B. Characterization of T-TENG based temperature sensor

Fig. 3(a) schematically shows the working principle of the developed T-TENG during one cycle. Fig. 3(b) plots the T-TENG output voltage with respect to temperature (five data points were taken between 25-90°C). The first output signal (red color) in Fig. 3(b) represents the output voltage of T-TENG at room temperature (i.e., 25°C). The fabricated tribo-negative layer (i.e., PTFE/conductive textile) was heated on a hotplate within the temperature range of 25-90°C, as shown in Fig. 3(b). After heating, the tribo-negative layer was attached to the TIRA shaker for TENG measurement and the temperature of the tribo-layer was confirmed by a thermal imager. The results in Fig. 3(b) are measured under 2 mm distance, 8 N applied force and 8 Hz operational frequency. Likewise, the T-TENG outputs were measured under other temperatures between 25 to 90°C. For a given temperature, the peak voltage in Fig. 3(b) is almost constant indicating equilibrium of TENG operation. The peak positive voltages are then taken from Fig. 3(b) and plotted against temperature in Fig. 3(c). The results indicate a TENG voltage output decreasing roughly linearly with increasing temperature ($R^2 > 0.99$). The sensitivity was calculated from the

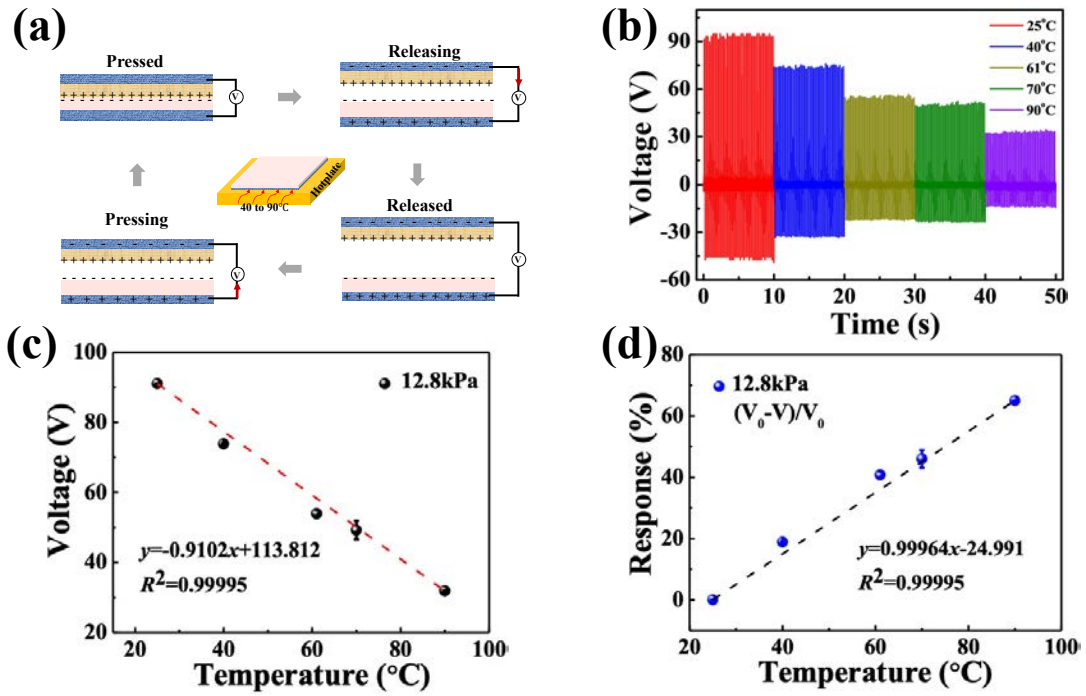

Fig. 3: Characterization of T-TENG based temperature sensor: (a) Working principle of the T-TENG based on Ar plasma treated PTFE and Nylon fabric, (b) T-TENG output voltage in the temperature range of 25-90 °C, (c) voltage versus temperature of the T-TENG device and (d) sensitivity of the T-TENG based self-powered temperature sensor.

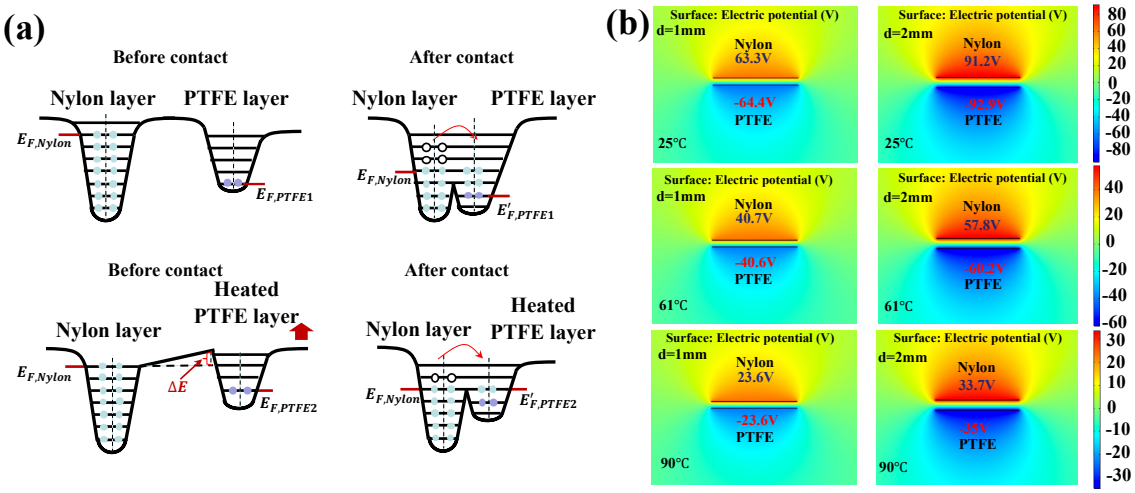

Fig. 4: (a) Overlapped electron cloud (OEC) model showing the electron transfer between interface pair for nylon and PTFE before or after heating and (b) COMSOL simulated potential distributions for the device at 25℃, 61℃, 90℃.

response of the device (i.e., $(V_0\text{-}V)/V_0$) in Fig. 3(d). The device sensitivity is the slope of the linear fitting line (i.e., ~1%/(℃)). The temperature induced changes in relative permittivity and density of traps could be the reason for observed change in TENG output [25]. Firstly, the reduction of relative permittivity of PTFE with increase in temperature reduces its ability to generate and store tribo-charges [25, 42]. Secondly, the generated surface tribo-charges include initial tribo-charges and 'sticky' tribo-charges. The previous studies indicate that the initial tribo-charges can be removed by thermal excitation, but 'sticky' tribo-charges cannot be detached by heating [43]. Thus, the effective defects on the PTFE surface (i.e., the escape of trapped charges in shallow traps and surface oxidation) are changed due to the perturbation of temperature [16, 25, 44, 45].

C. Overlapped electron-cloud (OEC) model analysis

To further explain the variation in output performance of T-TENG with change in the temperature of the PTFE layer, the overlapped electron-cloud (OEC) model is adopted [8, 46, 47]. The process of intrinsic electron transfer between two contact materials is described using this model. Fig. 4(a) schematically illustrates the electron transfer process for PTFE layer before and after heating using the OEC model. Accordingly, as shown in Fig. 4(a), the Fermi level of PTFE should be lower than nylon, because PTFE is more negative on the triboelectric series. Before PTFE contacts the nylon layer, the electron transfer is negligible, as there is no overlap between the electron clouds of these two materials. However, when they are in contact, their potential barrier is decreased, and this allows transfer of electrons from nylon to PTFE until their Fermi levels are balanced (i.e., $E'_{F,Nylon} = E'_{F,PTFE}$). After heating the PTFE layer, its Fermi level is expected to shift upwards (ΔE) due to escape of trapped charges in shallow traps. Briefly, the PTFE surface finds it more difficult to store the generated surface tribo-charges. The Fermi level of the nylon textile ($E_{F,Nylon}$) is fixed in each case. Thus, in this way, the high temperature changes the surface potential of the PTFE surface.

D. Simulation

The above hypothesis made using the OEC model was further confirmed using COMSOL finite element simulations. The surface potential was simulated at 25℃, 61℃ and 90℃ as shown in Fig. 4(b). Therein, the surface tribo-charge density was calculated by the measured transferred charges. The surface tribo-charge density was calculated at 25℃, 61℃ and 90℃ are 0.66, 0.37 and 0.25 C/m^2, respectively. These results indicate that the temperature has influenced PTFE's capability to obtain electrons from nylon during the contact electrification and this results in lower surface tribo-charge density on its surface as temperature increases. This conclusion agrees with the hypothesis in Fig. 4(a); namely, that temperature increases the potential barrier between PTFE and nylon (i.e., ΔE).

E. Characterization of multifunctional sensor system

The results shown in Fig. 3(c-d) were used to calculate the sensitivity of the presented device as a temperature sensor at a fixed 12.8 kPa applied pressure and 8Hz frequency. Further experiments were carried out to investigate the effects of pressure and frequency on the performance of the temperature sensor. Firstly, the results indicate that the TENG voltage output decreases roughly linearly with increasing temperature in Fig. 5(a-b). Fig. 5(a) shows the device output voltage under various pressures, when the PTFE layer was heated to different temperatures. The variation rate between the output voltage and temperature sensor was highest under 9.6 kPa applied pressure among three groups of measurements. From the results, it may be noted that the variation rate of the device is increased from 0.068 V/℃ to 0.32 V/℃ to 0.39 V/℃, after the applied pressure was increased from 3.2 kPa to 4.8 kPa to 9.6 kPa. Similarly with frequency, the highest variation rate was obtained at an operational frequency of 6 Hz as shown in Fig. 5(b). With increase in operational frequency, the variation rate improves from 0.066 V/℃ (2 Hz) to 0.23 V/℃ (4 Hz) to 0.44 V/℃ (6 Hz). These results show how the fabricated T-TENG responds to both temperature and mechanical (applied pressure or operational frequency) stimuli. Therefore, we modified the design of T-TENG to discriminate between the change in output voltage due to the perturbation of temperature or pressure. Thus,

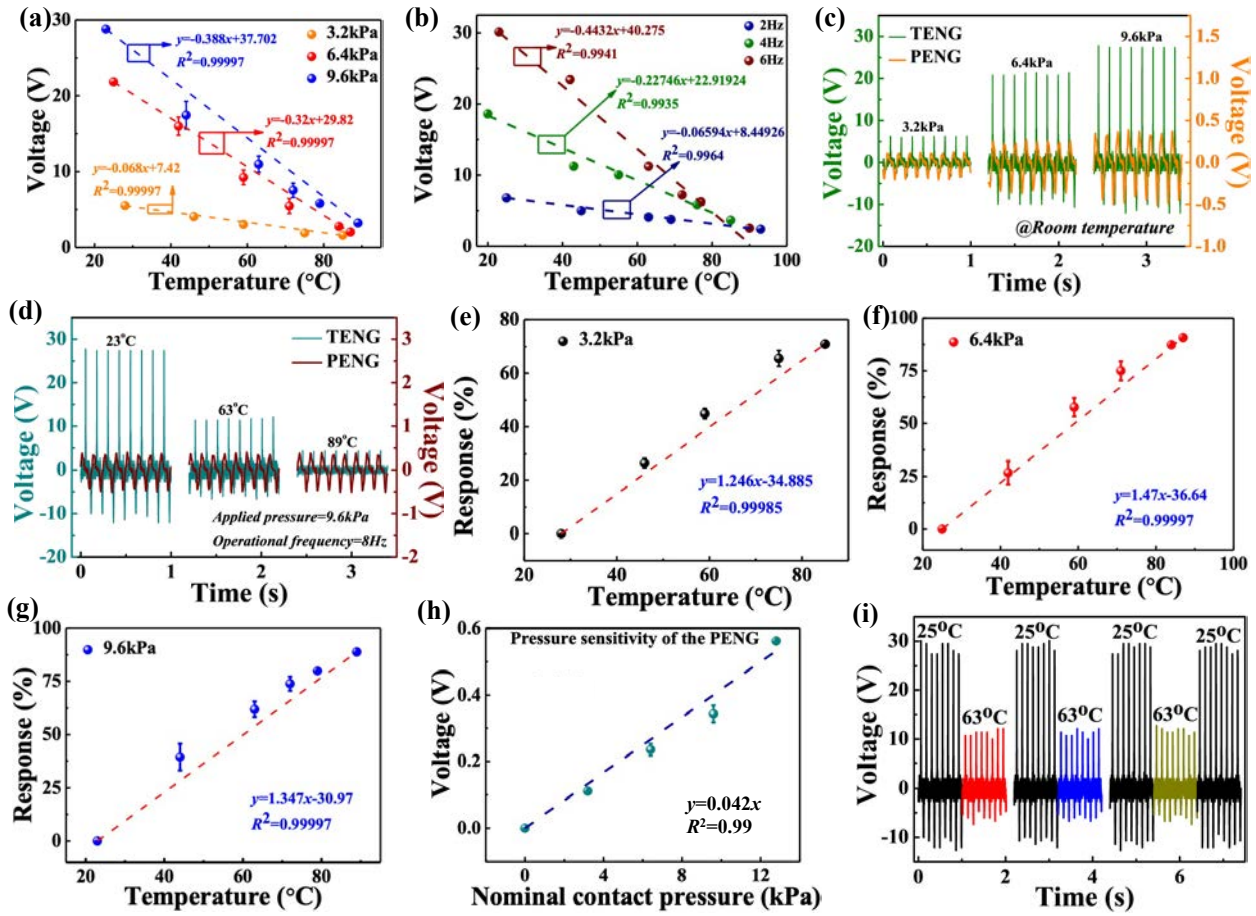

Fig. 5: Characterization of T-TENG and PENG based multifunctional device: (a) Output voltage versus temperature measured under 3.2, 6.4 and 9.6kPa contact pressure, (b) Output voltage versus temperature at 2, 4 and 6 Hz frequency, (c) separated output voltage signals for both T-TENG and PENG under 3.2, 6.4 and 9.6kPa, respectively, (d) separate output voltage signals of both T-TENG and PENG under 23, 63, 89℃ temperature. Sensitivities of the T-TENG based self-powered temperature sensor are given in (e-g) for contact pressures of (e) 3.2 kPa, (f) 6.4 kPa and (g) 9.6 kPa. PENG output voltage versus pressure is given in (h) and (i) illustrates the reusability of the T-TENG and PENG based multifunctional sensor system.

the new design can improve the practicability and accuracy of the T-TENG based temperature sensor. To achieve this, a PENG device was integrated on top of the nylon fabric layer to detect the applied pressure. A cellulose paper layer was placed in between the Nylon layer and the PENG to avoid the interference of temperature with the PENG outputs. Fig. 5(c) shows the output voltages from both TENG (green line) and PENG (yellow line) with both increasing with the increased applied pressure. However, when we fix the applied pressure and operational frequency (9.6 kPa and 8 Hz), but vary the temperature (Fig. 5(d)), only TENG output voltage (dark blue line) decreases from 29 V (25 ℃) to 13 V (63 ℃) to 4.9 V (89 ℃). Despite the increasing temperature of the PTFE layer, the PENG output voltages invariably remain stable at 0.43V (red line) in Fig. 5(d). Therefore, the sensitivity can be directly detected via calculating $(V_0\text{-}V)/V_0$ (i.e., response) where V_0 is the output voltage at room temperature and is the output voltage at the final temperature. Fig. 5(e-g) plots the response versus temperature under 3.2, 4.8 and 9.6 kPa applied pressure, respectively. The obtained sensitivities at the three pressure conditions are ~1.25, 1.5 and 1.35 %/℃, respectively. Fig. S1(a-c) shows the results at different operational frequencies. The results present the same situation as previous results. The obtained sensitivity (between response and temperature) under 2, 4, 6 Hz are ~0.93, 1.1 and 1.5 %/℃. The measurements are carried out at a fixed 9.6 kPa applied pressure. The output voltages of the PENG at different pressures are shown in Fig. 5(h). The PENG based pressure sensor exhibited a sensitivity of 0.042 V/kPa. Fig. 5(i) presents the reliability of the fabricated T-TENG based temperature sensor. After the temperature of PTFE decreases from 63℃ to room temperature, the output voltage changes back from 13 V to 29 V. The device reverts to its original voltages during multiple heating and cooling cycles confirming the reusability of the sensor. The developed T-TENG retained approximately 98% of the original output voltage in Fig. 2a after 8000 cycles of repeated vibration, as shown in Fig. S2. To the best of our knowledge, this is the first time a multifunctional self-powered textile sensor system integrating T-TENG and PENG technology has been developed to detect and discriminate between temperature and pressure. The presented T-TENG based self-powered temperature sensor can be used in various applications such as real-time temperature monitoring of a human body, breath monitoring and in robotics etc.

V. Conclusion

In summary, we have demonstrated a new self-powered temperature sensor based on a flexible textile triboelectric

nanogenerator (T-TENG). First, the performance of the T-TENG was optimized using plasma treatment. For this, the negative tribo-layer (PTFE film) was treated under different Ar plasma conditions (time varied from 3-12 min). The results demonstrated that there is a 10.2 times voltage increase from pristine to 12 min Ar plasma treated PTFE layers (150 W power). Simultaneously, the short circuit current density was found to increase by a factor of 9.2 for Ar plasma treated PTFE. T-TENGs based on a tribo-negative layer of 12 min Ar plasma treated PTFE in contact with Nylon fabric were then investigated for their temperature sensing capability. TENG voltage response was found to decrease linearly with increasing temperature exhibiting a sensitivity of ~ 1%/ (℃) for a temperature sensing regime between 25-90℃. In particular, a multifunctional sensor system integrating a PENG sensor with a T-TENG has been fabricated with the capability to detect and distinguish between the effect of pressure and temperature on TENG output. The output voltage of the T-TENG at various temperatures were repeatedly tested under 3.2, 4.8 and 9.6 kPa pressure and a sensitivity of ~ 1.25, 1.5 and 1.35%/ ℃ , respectively was obtained for the temperature sensor. This design offers a possible route to use T-TENG as a self-powered wearable temperature sensor which can correct for pressure induced changes. This self-powered temperature sensor also opens avenues for several applications such as autonomously detecting temperature in the human body or in self-powered e-Skin for the gloves of humanoid robots etc.

REFERENCES

[1] Iqbal, S.M.A., Mahgoub, I., Du, E. *et al*., Advances in healthcare wearable devices. *Npj. Flex. Electron.*, vol. 5, pp. 1-9, 2021.

[2] Bayoumy, K., Gaber, M., Elshafeey, A. *et al.*, Smart wearable devices in cardiovascular care: where we are and how to move forward. *Nat. Rev. Cardiol.*, vol. 18, pp. 581–599, 2021.

[3] O. Ozioko and R. Dahiya, "Smart Tactile Gloves for Haptic Interaction, Communication, and Rehabilitation," *Advanced Intelligent Systems,* p. 2100091, 2021.

[4] J. Neto, R. Chirila, A. S. Dahiya, A. Christou, D. Shakthivel, R. Dahiya, “Skin Inspired Thermoreceptors based electronic skin for Biomimicking Thermal Pain Reflexes,” *Adv. Sci.*, 2201525, 2022.

[5] F. Liu, S. Deswal, A. Christou, Y. Sandamirskaya, M. Kaboli, R. Dahiya, “Neuro-inspired e-Skin for Robots,” *Sci. Robot.*, Vol. 7, abl7344, 2022.

[6] F. Liu, S. Deswal, A. Christou, R. Chirila, M. S. Baghini, D. Shakthivel, M. Chakraborty, R. Dahiya, “Printed synaptic transistor–based electronic skin for robots to feel and learn,” *Sci. Robot.*, Vol 7, eabl7286, 2022

[7] J. Zhu, M. Zhu, Q. Zhi *et al.*, “Progress in TENG technology—A journey from energy harvesting to nanoenergy and nanosystem,” *EcoMat*, Vol 2, e12058, pp. 1-45, 2020.

[8] G. Min *et al.*, "Ferroelectric-assisted high-performance triboelectric nanogenerators based on electrospun P (VDF-TrFE) composite nanofibers with barium titanate nanofillers," *Nano Energy,* vol. 90, p. 106600, 2021.

[9] R. Mukherjee, P. Ganguly, and R. Dahiya, "Bioinspired distributed energy in robotics and enabling technologies," *Advanced Intelligent Systems,* p. 2100036, 2021.

[10] C. G. Núñez, L. Manjakkal, and R. Dahiya, "Energy autonomous electronic skin. *NPJ. Flex. Electron.,* Vol 3," 2019.

[11] G. Khandelwal, R. Dahiya, “Self-Powered Active Sensing based on Triboelectric Generator,” *Adv. Mater.*, Vol 34 (33), 2200724, 2022.

[12] G. Min, Y. Xu, P. Cochran, N. Gadegaard, D. M. Mulvihill, and R. Dahiya, "Origin of the contact force-dependent response of triboelectric nanogenerators," *Nano Energy,* vol. 83, p. 105829, 2021.

[13] R. Zhang and H. Olin, "Material choices for triboelectric nanogenerators: a critical review," *EcoMat,* vol. 2, no. 4, p. e12062, 2020.

[14] Y. J. Kim, J. Lee, S. Park, C. Park, C. Park, and H.-J. Choi, "Effect of the relative permittivity of oxides on the performance of triboelectric nanogenerators," *RSC adv.,* vol. 7, no. 78, pp. 49368-49373, 2017.

[15] Y. S. Zhou *et al.*, "In situ quantitative study of nanoscale triboelectrification and patterning," *Nano lett.,* vol. 13, no. 6, pp. 2771-2776, 2013.

[16] B. Cheng *et al.*, "High performance temperature difference triboelectric nanogenerator," *Nat. Commun.,* vol. 12, no. 1, pp. 1-8, 2021.

[17] H. Zou *et al.*, "Quantifying the triboelectric series," *Nat. Commun.,* vol. 10, no. 1, pp. 1-9, 2019.

[18] S. Wang *et al.*, "Maximum surface charge density for triboelectric nanogenerators achieved by ionized‐air injection: methodology and theoretical understanding," *Adv. Mater.,* vol. 26, no. 39, pp. 6720-6728, 2014.

[19] T. Prada *et al.*, "Enhancement of output power density in a modified polytetrafluoroethylene surface using a sequential O2/Ar plasma etching for triboelectric nanogenerator applications," *Nano Res.,* vol. 15, no. 1, pp. 272-279, 2022.

[20] Y. Momose, Y. Tamura, M. Ogino, S. Okazaki, and M. Hirayama, "Chemical reactivity between Teflon surfaces subjected to argon plasma treatment and atmospheric oxygen," *Journal of Vacuum Science & Technology A: Vacuum, Surfaces, and Films,* vol. 10, no. 1, pp. 229-238, 1992.

[21] X.-J. Shao, G.-J. Zhang, J.-Y. Zhan, and G.-M. Xu, "Research on surface modification of polytetrafluoroethylene coupled with argon dielectric barrier discharge plasma jet characteristics," *IEEE Trans Plasma Sci.,* vol. 39, no. 11, pp. 3095-3102, 2011.

[22] C. Wang, J.-r. Chen, and R. Li, "Studies on surface modification of poly (tetrafluoroethylene) film by remote and direct Ar plasma," *Appl. Surf. Sci.,* vol. 254, no. 9, pp. 2882-2888, 2008.

[23] Y. Xu, G. Min, N. Gadegaard, R. Dahiya, and D. M. Mulvihill, "A unified contact force-dependent model for triboelectric nanogenerators accounting for surface roughness," *Nano Energy,* vol. 76, p. 105067, 2020.

[24] G. Min, A. S. Dahiya, D. M. Mulvihill, and R. Dahiya, "A wide range self-powered flexible pressure sensor based on triboelectric nanogenerator," in *2021 IEEE International Conference on Flexible and Printable Sensors and Systems (FLEPS)*, 2021: IEEE, pp. 1-4.

[25] C. X. Lu *et al.*, "Temperature effect on performance of triboelectric nanogenerator," *Advanced Engineering Materials,* vol. 19, no. 12, p. 1700275, 2017.

[26] J.-H. Seo, K. Zhang, M. Kim, W. Zhou, and Z. Ma, "High-performance flexible BiCMOS electronics based on single-crystal Si nanomembrane," *NPJ. Flex. Electron.,* vol. 1, no. 1, pp. 1-7, 2017.

[27] K. Dong, X. Peng, and Z. L. Wang, "Fiber/fabric‐based piezoelectric and triboelectric nanogenerators for flexible/stretchable and wearable electronics and artificial intelligence," *Adv. Mater.,* vol. 32, no. 5, p. 1902549, 2020.

[28] Y. Su *et al.*, "Improving sensitivity of self-powered room temperature NO_2 sensor by triboelectric-photoelectric coupling effect," *Appl. Phys. Lett.,* vol. 115, no. 7, p. 073504, 2019.

[29] Y. Kumaresan, G. Min, A. S. Dahiya, A. Ejaz, D. Shakthivel, and R. Dahiya, "Kirigami and Mogul‐Patterned Ultra‐Stretchable High‐Performance ZnO Nanowires‐Based Photodetector," *Adv. Mate. Technol. ,* vol. 7, no. 1, p. 2100804, 2022.

[30] S. Wang, L. Lin, and Z. L. Wang, "Triboelectric nanogenerators as self-powered active sensors," *Nano Energy,* vol. 11, pp. 436-462, 2015.

[31] K. Xia, Z. Zhu, H. Zhang, and Z. Xu, "A triboelectric nanogenerator as self-powered temperature sensor based on PVDF and PTFE," *Appl. Phys. A,* vol. 124, no. 8, pp. 1-7, 2018.

[32] Y. Wang, L. Zhang, and A. Lu, "Highly stretchable, transparent cellulose/PVA composite hydrogel for multiple sensing and triboelectric nanogenerators," *J. Mater. Chem. A,* vol. 8, no. 28, pp. 13935-13941, 2020.

[33] J. Rao *et al.*, "Tactile electronic skin to simultaneously detect and distinguish between temperature and pressure based on a triboelectric nanogenerator," *Nano Energy,* vol. 75, p. 105073, 2020.

[34] G. Min *et al.*, "Textile Triboelectric Nanogenerators as Self Powered Wearable Temperature Sensors," 2022 IEEE International Conference on Flexible and Printable Sensors and Systems (FLEPS), 2022, pp. 1-4.

[35] H. H. Singh and N. Khare, "Flexible ZnO-PVDF/PTFE based piezo-tribo hybrid nanogenerator," *Nano Energy,* vol. 51, pp. 216-222, 2018.

[36] D. S. Kong, J. Y. Han, Y. J. Ko, S. H. Park, M. Lee, and J. H. Jung, "A highly efficient and durable kirigami triboelectric nanogenerator for rotational energy harvesting," *Energies,* vol. 14, no. 4, p. 1120, 2021.
[37] V. U. Somkuwar, A. Pragya, and B. Kumar, "Structurally engineered textile-based triboelectric nanogenerator for energy harvesting application," *J. MATER. SCI.,* vol. 55, no. 12, pp. 5177-5189, 2020.
[38] X. He, H. Zou, Z. Geng, X. Wang, W. Ding, F. Hu, Y. Zi, C. Xu, S. L. Zhang, H. Yu, M. Xu, W. Zhang, C. Lu, and Z. L. Wang, "A hierarchically nanostructured cellulose fiber-based triboelectric nanogenerator for self-powered healthcare products," *Advanced Functional Materials,* vol. 28, no. 45, p. 1805540, 2018.
[39] H. Li, S. Zhao, X. Du, J. Wang, R. Cao, Y. Xing, and C. Li, "A compound yarn based wearable triboelectric nanogenerator for self-powered wearable electronics," *Advanced Materials Technologies*, vol. 3, no. 6, p. 1800065, 2018.
[40] S. S. Kwak, H. Kim, W. Seung, J. Kim, R. Hinchet, and S.-W. Kim, "Fully Stretchable Textile triboelectric nanogenerator with knitted fabric structures," *ACS Nano*, vol. 11, no. 11, pp. 10733–10741, 2017.
[41] T. Zhou, C. Zhang, C. B. Han, F. R. Fan, W. Tang, and Z. L. Wang, "Woven structured triboelectric nanogenerator for wearable devices," *ACS Applied Materials & Interfaces,* vol. 6, no. 16, pp. 14695–14701, 2014.
[42] P. Ehrlich, L. Amborski, and R. Burton, "Dielectric properties of teflon from room temperature to 314 C and from frequencies of 102 to 105 c/s," *J. Res. Nat. Bur. Stand,* vol. 51, pp. 185-188, 1953.
[43] S. Lin, L. Xu, A. Chi Wang, and Z. L. Wang, "Quantifying electron-transfer in liquid-solid contact electrification and the formation of electric double-layer," *Nature Communications*, vol. 11, no. 1, 2020.
[44] Z. L. Wang and A. C. Wang, "On the origin of contact-electrification," *Mater. Today,* vol. 30, pp. 34-51, 2019.
[45] M. Olsen, J. Örtegren, R. Zhang, S. Reza, H. Andersson, and H. Olin, "Schottky model for triboelectric temperature dependence," *Sci. Rep.,* vol. 8, no. 1, pp. 1-5, 2018.
[46] J. S. C. Koay, W. C. Gan, A. E. Soh, J. Y. Cheong, K. C. Aw, and T. S. Velayutham, "An overlapped electron-cloud model for the contact electrification in piezo-assisted triboelectric nanogenerators via control of piezoelectric polarization," *J. Mater. Chem. A,* vol. 8, no. 48, pp. 25857-25866, 2020.
[47] C. Xu *et al.*, "On the electron - transfer mechanism in the contact - electrification effect," *Adv. Mater.,* vol. 30, no. 15, p. 1706790, 2018.

Guanbo Min received a B.Sc. degree in Electronic Information Technology from Macau University of Science and Technology, Macao S.A.R, China in 2015 and a M.Sc. degree in Electronics and Electrical Engineering from University of Glasgow in 2017. In 2022, he obtained his Ph.D. degree in mechanical engineering at University of Glasgow. Afterward, he is a post-doctoral researcher in the Bendable Electronics and Sensing Technologies (BEST) at the University of Glasgow. His research interests are focused on flexible and wearable energy harvesters and their applications in self-powered sensors, self-powered or self-charging system.

Gaurav Khandelwal is currently working as a post-doctoral fellow in the Bendable Electronics and Sensing Technologies (BEST) research group at the University of Glasgow. He completed his Ph.D. (with excellence) from the Department of Mechatronics Engineering at Jeju National University, South Korea, where he received the Brain Korea fellowship. He holds a Bachelor's and Master's degree in Nanotechnology from the Centre for Converging Technologies, U.O.R, India. He worked as Project Associate at the Indian Institute of Technology (IIT), Delhi, India. He also worked as a research intern in the field of peptide-based nanofibers at the Institute of Nano Science and Technology (INST), India. His current research area includes triboelectric nanogenerators, piezoelectric nanogenerators, self-powered sensors, and nanomaterial synthesis and characterization.

Abhishek S. Dahiya is Research Associate in Bendable Electronics and Sensing Technologies (BEST) group at the University of Glasgow. He received Ph.D. from the GREMAN laboratory, Université François Rabelais de Tours, France in 2016. He has done postdoctoral work at various CNRS laboratories in France: GREMAN (2016- 2017), ICMCB (2018-2019), and IES/LIRMM (2019-2020). His research interest includes synthesis of nanomaterials, nanofabrication, energy harvesting, and printed and flexible electronics.

Daniel M. Mulvihill is Senior Lecturer (Associate Professor) in Mechanical Engineering at University of Glasgow. He completed a D.Phil. in Engineering Science at the University of Oxford in 2012 and subsequently undertook postdoctoral periods at the University of Limerick, EPFL Switzerland and the University of Cambridge prior to joining Glasgow in 2016. His interests are mainly focused on materials engineering and tribology. Dr Mulvihill is a former Institution of Mechanical Engineers (IMechE) Tribology Trust Bronze Medalist (2013). He presently leads a major £1.5M EPSRC project (EP/V003380/1) on next generation textile triboelectric nanogenerators. He is as Associate Editor of Results in Engineering (Elsevier) and Novel Materials Editor at Chemical Engineering Journal (Elsevier).

Ravinder Dahiya (Fellow, IEEE) is the leader of Bendable Electronics and Sensing Technologies (BEST) research group. His group conducts fundamental and applied research in flexible and printable electronics, tactile sensing, electronic skin, robotics, and wearable systems. He has authored or co-authored more than 450 publications, books and submitted/granted patents and disclosures. He has led several international projects. He is President (2022-23) of the IEEE Sensors Council. He is the Founding Editor in Chief of IEEE JOURNAL ON FLEXIBLE ELECTRONICS (J-FLEX) and has served on the editorial boards of Scientific Report, IEEE SENSORS JOURNAL (2012-2020) and IEEE TRANSACTIONS ON ROBOTICS (2012-2017). He was the Technical Program co-chair of IEEE Sensors 2017 and IEEE Sensors 2018 and has been General Chair of several conferences including IEEE FLEPS (2019, 2020, 2021), which

he founded in 2019. He holds the prestigious EPSRC Fellowship and received in past the Marie Curie and Japanese Monbusho Fellowships. He has received several awards, including 2016 Microelectronic Engineering Young Investigator Award (Elsevier), 2016 Technical Achievement Award from the IEEE Sensors Council and 12 best paper awards as author/coauthor in International Conferences and Journal.